ARMA 13-479

Inferring Mine Floor Properties from Pillar Size and Floor Heave

Tesarik, D.R., Whyatt, J.K. and Larson, M.K.

Office of Mine Safety and Health Research, National Institute for Occupational Safety and Health, Spokane, WA, U.S.A.

ABSTRACT: Consistency between actual in-mine and modeled ground response to mining is essential if a model is to be used as a mine design tool. A new procedure is presented in this paper that infers Mohr-Coulomb floor properties that will synchronize floor heave behavior between mine and model. The procedure works where the presence of floor heave depends on pillar size, as has been observed in a deep western U.S. longwall coal mine. In this case, floor heave was observed near pillars approximately 52.4 m (172 ft) wide but was absent around pillars approximately 23 m (76 ft) wide, as the longwall passed. Pillars were idealized in FLAC3D models as a single square column that includes the roof, pillar, and floor. Coal in mine pillars was modeled as a Hoek-Brown material with parameters tuned to match one of Bieniawski's in situ compression tests, scaled to an unconfined compressive strength of 6.2 MPa (900 psi). Models of various pillar shapes replicated Bieniawski pillar strength equation estimates for pillar width-to-height ratios up to 8. Mohr-Coulomb properties in the floor were then varied to define a boundary between heave and no-heave floor response to loading for each pillar size. The intersection of these solution sets served to bound Mohr-Coulomb properties for the mine floor. A representative set of properties within this region reduced capacity of the 52.4-m (172-ft) wide pillar, which has a width-to-height ratio of 17, by 46% compared to a linear extrapolation of Bieniawski's equation. Pillar capacities with inferred floor properties are easily fit to the Holland-Gaddy and Maleki empirical equations. This procedure provides an alternative, and significantly different, extrapolation of coal pillar capacity that correctly models observed entry behavior, yet requires only careful observation to ascertain.

1. INTRODUCTION

Design of safe mine openings rests in part upon an understanding of the strength of geologic materials that compose supporting pillars. This paper was developed as part of an effort by the Office of Mine Safety and Health Research (OMSHR) of the National Institute for Occupational Safety and Health to improve the quality of these strength estimates for deep longwall coal mines. These mines are operating deeper, and in different geologic regimes, than those studied in development of popular pillar design methods [1, 2]. OMSHR is conducting a detailed study of pillar strength and loading in one of these mines to address this gap. The study included visual observation of gateroad pillar and entry response to loads induced by the approaching longwall [3]. Visual observations were rated on a scale similar to that suggested by Karabin and Evanto [4] and published as general guidelines in U.S. Department of Labor Program Information Bulletin No. P09-03 [5]. Ratings showed that floor heave with longwall advance differed markedly with pillar size in two adjacent gateroads during mining of the first panel of a new district. Floor heave was abundant near pillars approximately 52.4 m (172 ft) wide but not observed near pillars approximately 23 m (76 ft) wide, as shown in Figure 1.

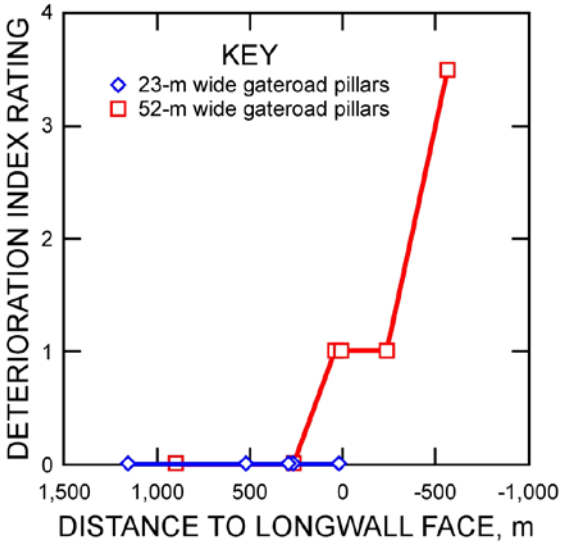

Fig. 1. Floor deterioration ratings in the middle entry relative to longwall face position (after Lawson, et al. [3]).

The contrast in floor response to mining of the same panel, dependent only on pillar size, was fortuitously similar to a controlled experiment. Common pillar and pillar foundation equations, such as those by Bienawski [6] (Eq. 1) and Vesic [7], respectively, describe increasing pillar strength with width. An adaption of Vesic's equation by Speck has been used extensively in the Illinois coal basin for decades and recently critically examined by Gadde [8]. The Bieniawski equation is:

$$P = UCS(0.64 + 0.36\frac{w}{h}) \qquad (1)$$

Where:

P = average pillar capacity,

UCS = unconfined compressive strength of a coal cube with side length = 1.5 m (5 ft),

w = width of a square pillar, and

h = height of a square pillar

One interesting characteristic of these equations is that pillar strength increases more quickly with width than foundation strength. Thus, for particular combinations of materials strengths, there can be a crossover where the floor replaces the pillar in limiting system strength, as shown in Figure 2. As an example, 23-m (76-ft) wide and 52.4-m (172-ft) wide pillars with 3 m (10 ft) seam heights have width to height ratios of 7.7 and 17.5, respectively. For the floor properties given for Figure 2 pillar strength is less than floor strength for the intermediate pillar, resulting in vertical deformation primarily in the pillar with limited floor deformation. On the contrary, pillar strength exceeds floor strength for the squat pillar, which would induce floor heave.

Situations where pillar capacity is limited by a weak floor are well known [9]. The pillar shape where this crossover occurs would appear to provide insight into relative strength of floor and pillar materials. Such insight could reduce the need to sample and test weak floor materials that can be difficult to sample, transport, and prepare for testing [10]. Scoping models showed that pillar systems near this crossover point activate failure mechanisms that include both floor and rib, complicating the analysis. Still, the concept proved to be a sound basis for this modeling study.

Based on the above concept, this study was designed to examine if visual observations of varying gateroad floor behavior with gateroad pillar size could be used to gain insight into, or even bound, properties of the floor relative to pillars—that is, given coal pillar properties and floor heave observations, what can we deduce about floor properties?

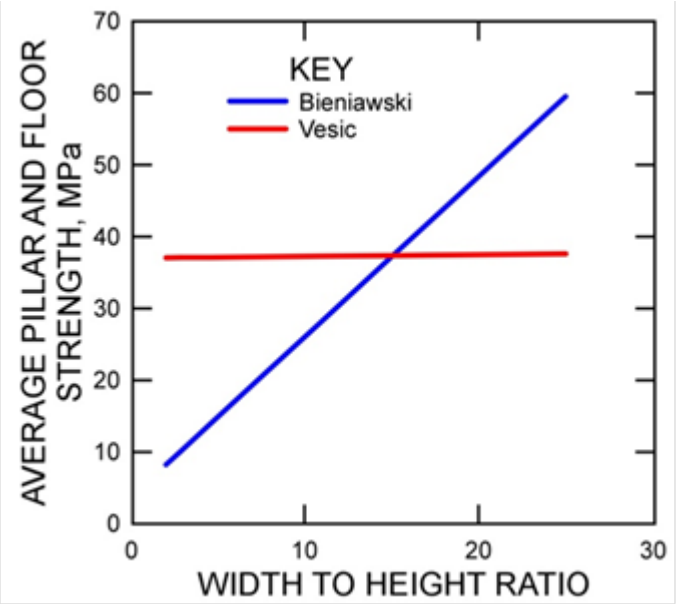

Fig. 2. Average pillar and floor strength for floor cohesion = 3.4 MPa (500 psi), floor angle of internal friction = 5°, floor specific density = 2195 kg/m3 (137 lb/ft3), and pillar unconfined compressive strength = 6.2 MPa (900 psi) as estimated by the Bieniawski and Vesic equations, respectively.

2. STUDY DESIGN

The first challenge in designing this study was to simplify matters sufficiently to capture the interaction of entry floor and pillar rib while avoiding the complexity of modeling a longwall panel. The resulting course was inspired by boundary element methods for panel analysis, including LaModel [11] and MulSim/NL [12]. These models use force-displacement curves representative of coal pillars, or portions of pillars. These curves are derived separately, possibly from numerical models but more often from the Bieniawski pillar capacity formula [6]. Thus, the problem scope can be reduced to a study of the force-displacement characteristics of the pillar system (roof-pillar-floor).

This simplification introduces symmetry, reducing the model to a quarter of a pillar, which was meshed in FLAC3D [13] as shown in Figure 3. The roof was meshed with 3-, 3.7-, 14.6-, and 26.8-m (10-, 12-, 48- and 88-ft) thick zones of elastic rock above the seam with side lengths of 0.3, 0.6, 1.2, and 2.4 m (1, 2, 4, and 8 ft), respectively, as shown in Figure 3. The mine floor was symmetrical through the 1.2-m (4-ft) zones. The 2.4-m (8-ft) zone layer was increased to 78-m (256-ft) thick to allow general floor deformation. Load was applied by a constant boundary velocity boundary condition at the top of the mesh of 2.54×10^{-6} m/s (0.0001 in/s).

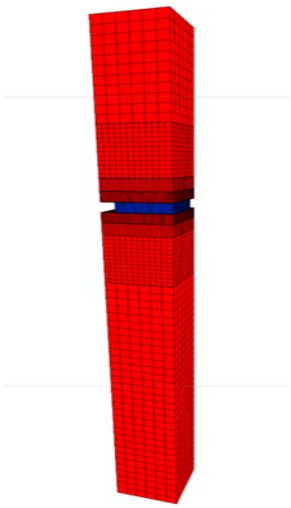

Fig. 3. FLAC3D mesh for 23-m (76-ft) wide pillar with 6 m (20 ft) entries represented in quarter symmetry. Brick width at mesh top and bottom is 2.4 m (8 ft).

Coal pillar strength estimates provided by the Bienawski equation had to be replicated in the model by a strength criterion, preferably one that reflects the nonlinear relationship between strength and confining pressure typically found in coal [14]. A number of such strength envelopes have been used. Scovazzo [15], for example, reports that Carter's strength envelope often provides the best match to coal test data. Kalamaras and Bieniawski [16] prefer the Generalized Bieniawski criterion, citing its lack of tensile strength, which they consider to be uncertain.

As a practical matter, though, the Hoek-Brown strength criterion [17] (Eq. 2) is much more likely to be available in modeling programs and thus, is often used. The Hoek-Brown equation relates strength to confining pressure as:

$$\sigma_1 = \sigma_3 + \sigma_c \left(m \frac{\sigma_3}{\sigma_c} + s \right)^a \qquad (2)$$

Where:

σ_1 = strength

σ_3 = least confining stress,

σ_c = uniaxial compressive strength of intact rock, and

m, s, and a = empirically derived parameters

For instance, Duncan Fama et al. [18] calibrated Hoek-Brown parameters to pillar strength formulas of Bieniawski and Van Heerden [6], Obert and Duvall [19], and Salamon and Monroe [20]. Many of these studies augment strength criteria with strain softening schemes [21, 22]. Esterhuizen et al. [23] calibrated Hoek-Brown parameters with in situ stress measurements in a coal pillar rib as well as pillar capacities from Bieniawski's pillar capacity equation.

Our model uses a strain softening Hoek-Brown strength law fit to an experiment. In this case, an experiment underlying the Bieniawski equation, scaled in strength as recommended for U.S. pillar design [1, 24]. The roof is kept elastic with typical sandstone properties for this calibration with 20.68 GPa ($3x10^6$ psi) for modulus [25], 2595 kg/m^3 (162 lb/ft^3) for specific density, and 0.25 for Poisson's ratio. Modulus and specific density are reduced to values consistent with the lower range of laboratory modulus values for shale [26] when pillar and floor interaction are explored. These properties are 9.79 GPa (1.42 x 10^6 psi) for modulus and 2195 kg/m^3 (137 lb/ft^3) for specific density.

Three types of floor properties were used. In the first case, an elastic floor with the above sandstone properties was used to calibrate Hoek-Brown parameters. In the second, the floor was modeled as a Mohr-Coulomb material for exploring floor strength, following Vesic in our conceptual example and Wilson's [27] pillar model (although Wilson considered a Mohr-Coulomb interface rather than a mass). These runs used the above shale properties. The floor properties remained the same for the two pillar sizes that were investigated in this case. There were no stratigraphic data available at depth below the coal seam, thus it is assumed that the composite behavior of the floor beneath the two pillar sizes was reasonably similar. Third, an exploration of coal pillar behavior in "strong" strata late in the paper used the above sandstone properties along with 5 MPa (725 psi) cohesion and 30^o friction.

3. COAL HOEK-BROWN PARAMETERS

The first task in this numerical experiment is to discern Hoek-Brown parameters of Eq. (2) [17] for the coal pillar. As discussed previously, parameters in a FLAC3D pillar model were adjusted (calibrated) until a stress versus strain plot matched an experimental curve. In this case, a scaled stress versus strain plot from one of Bieniawski's in situ unconfined compression tests with width-to-height ratio of 2.78 [6]. Experimental stresses were halved to adjust coal strength to the 6.2 MPa (900 psi) recommended by Mark and Barton [2], for use with the Bieniawski pillar capacity equation (Eq. 1) in U.S. coal mines. Thus, the 20.6 MPa (2985 psi) capacity of Bieniawski's in situ pillar was reduced to 10.2 MPa (1475 psi) for the target curve; a capacity consistent with Bieniawski's equation (Eq. 1) with a 6.2 MPa (900 psi) UCS and width-to-height ratio of 2.78.

Calibration assumed that deformation and failure in the reference test were driven primarily by coal behavior. Calibration of coal properties was pursued through a number of models, starting with an initial guess and adjusting to match the scaled experimental curve. The

resulting stress-strain plot with Hoek-Brown coal properties of Table 1 is shown in Figure 4 along with experimental, and scaled experimental, data.

Table 1. Parameters for Hoek-Brown constitutive equation calibrated to Bieniawski's in situ unconfined compression test

Parameter	Value
UCS (laboratory scale)	20.3 MPa (2950 psi)
Young's modulus	3.79 GPa (550 ksi)
Poisson's ratio	0.25
a	0.65
m	1.47
m, residual	0.36
s	0.07
s, residual	0.001
Peak-to-residual strain	0.051

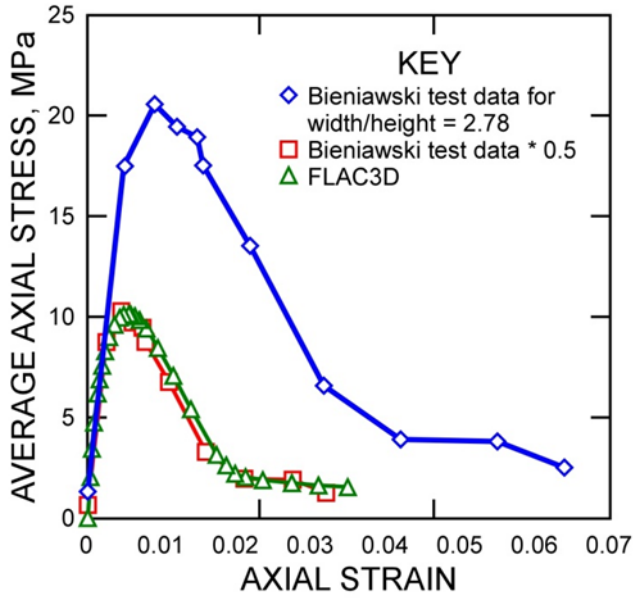

Fig. 4. Experimental, re-referenced, and model curves showing average pillar stress versus strain for width-to-height of 2.78.

4. PILLAR AND FLOOR INTERACTION

Interaction of pillar and floor was explored using the calibrated coal model with floors having various strength parameters. The degree and characteristics of floor heave that could be readily observed in operating mines were of particular interest. Floor deformation was present in virtually all models, at least to some degree—but not always to a degree that would be readily apparent to an underground observer. Thus, floor heave had to be defined carefully although any such definition is arbitrary. We chose to define heave as a distortion of the floor where vertical displacement at one point exceeded another by 3.8 cm (1.5 in). Any models run to 0.9 m (3 ft) of pillar shortening at the rib (roughly 30% strain) without floor heave meeting this definition were designated as having no floor heave.

Floor strength parameters were varied systematically in a number of case study models. Results were used to create a "map" of floor behavior in floor strength space for each of the two pillars. The goal was to define a floor strength parameter region that would replicate floor deformation observations for both squat and intermediate size pillars. Six of these cases, representing typical floor behavior in these regions, are described in some detail here. The overall map is developed in the following section.

4.1 Case 1: Intermediate pillar, floor USC of 5.95 MPa (863 psi), cohesion of 2.59 MPa (375 psi), friction angle of 8 Degrees

This weak floor case for cohesion of 2.59 MPa (375 psi) and friction angle of 8 degrees produced floor heave around 23-m (76-ft) wide pillars but floor heave was not observed in the field for this size pillar. Thus, this case serves to bound floor strength on the weak side. Even so, the onset of visual floor heave did not occur until the softening stage of pillar deformation (Figure 5). The progression of floor heave in this case is sporadic—increasing, decreasing, and increasing again.

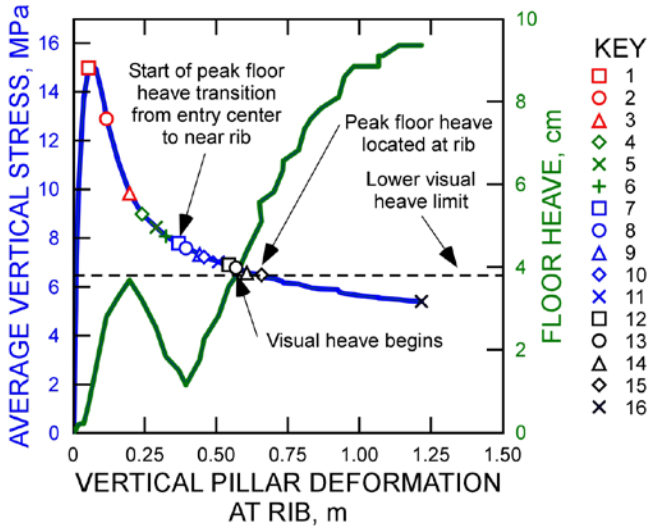

Fig. 5. Floor heave and average vertical stress versus vertical pillar deformation for a 23-m (76-ft) wide pillar. Floor properties were 2.59 MPa (375 psi) for cohesion, 8° for angle of internal friction, and 9.79 GPa (1.42 x 10^6 psi) for Young's modulus.

Net floor displacements are plotted at indicated points on the pillar deformation curve in Figure 6. These curves show how the floor displacement profile evolves across the entry floor and under the pillar. According to our definition, floor heave would be visually detectable for a person standing in the center of the entry when pillar closure at the rib is about 0.6 m (2 ft) (roughly 20% pillar shortening).

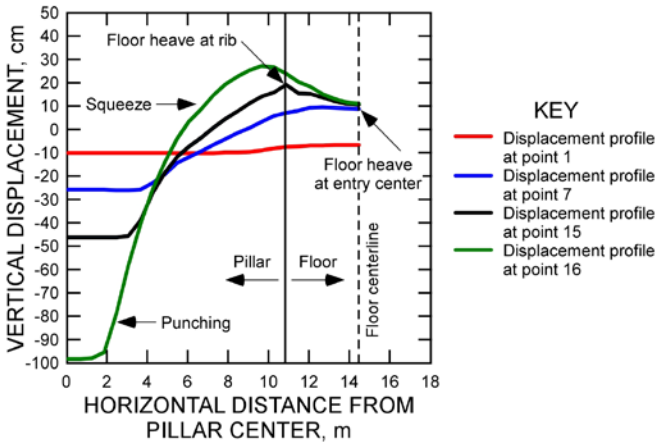

Fig. 6. Vertical displacement of pillar and floor relative to initial floor level for a 23-m (76-ft) wide pillar. Floor properties were 2.59 MPa (375 psi) for cohesion, 8° for angle of internal friction, and 9.79 GPa (1.42 x 10^6 psi) for Young's modulus.

Floor displacements are referenced to the observer's feet at entry center in Figure 7 to show how the distribution of floor deformation would appear to an observer. The location of maximum floor heave moves from the entry center to near the rib with continued pillar deformation. Thus, in this particular case, progression of the pillar along its load-deformation curve might be traced by observation.

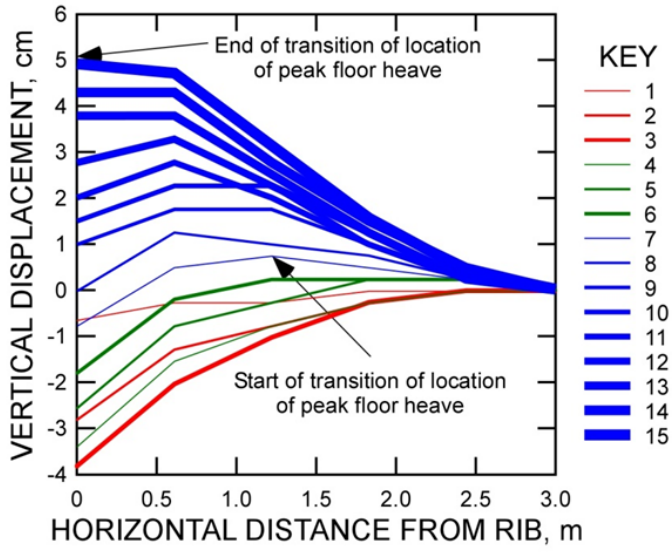

Fig. 7. Vertical displacement of floor adjacent to a 23-m (76-ft) wide pillar as viewed from center of entry. Floor properties were 2.59 MPa (375 psi) for cohesion, 8° for angle of internal friction, and 9.79 GPa (1.42 x 10^6 psi) for Young's modulus.

4.2 Case 2: Intermediate pillar, floor UCS of 8.22 MPa (1192 psi), cohesion of 3.4 MPa (500 psi), friction angle of 10 degrees

The evolution of floor behavior around intermediate pillars was tested further with a slight strengthening of the floor for cohesion of 3.4 MPa (500 psi) and a friction angle of 10 degrees. This run was aimed at defining a floor strength region where the floor would not heave around these pillars. This run showed minor heave that did not arise to the level of our definition which is 3.8 cm (1.5 in) (Figure 8).

4.3 Case 3: Squat pillar, floor UCS of 25.58 MPa (3710 psi), cohesion of 11.72 MPa (1700 psi), low friction angle of 5 degrees

Floor heave adjacent to a squat 52.4-m (172-ft wide) pillar with floor properties of 11.72 MPa (1700 psi) for cohesion and 5° for angle of internal friction is shown in Figure 9. Floor heave initiated near average peak pillar stress but would not be visually detectable until rib closure is equal to about 76 cm (30 in). The location of the highest point of floor heave starts and remains at the rib-floor interface as shown in Figure 10. Average vertical pillar stress for each floor profile in Figure 10 is identified in Figure 9.

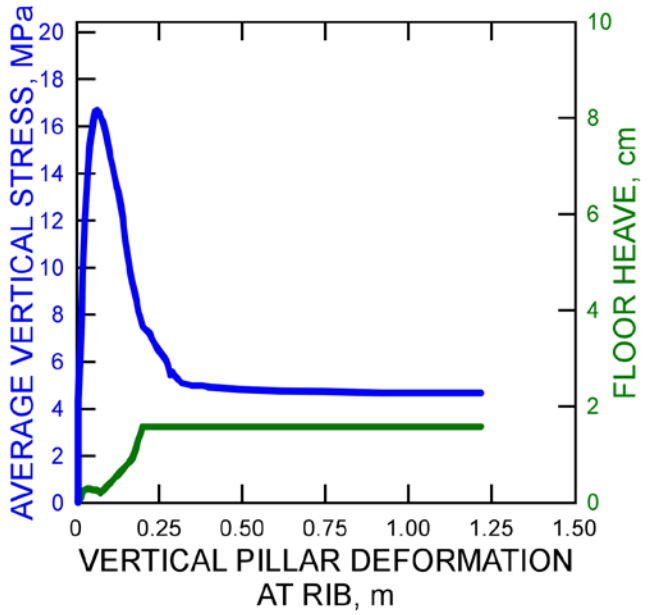

Fig. 8. Average vertical stress and floor heave plotted against vertical pillar deformation for a 23-m (76-ft) wide pillar. Floor properties were 3.4 MPa (500 psi) for cohesion, 10° for angle of internal friction, and 9.79 GPa (1.42 x 10^6 psi) for Young's modulus.

4.4 Case 4: Squat pillar, floor UCS of 9.85 MPa (1428 psi), cohesion of 3.4 MPa (500 psi), friction angle of 20 degrees

Floor heave adjacent to a 52.4-m (172-ft) wide pillar with floor properties of 3.4 MPa (500 psi) for cohesion and 20° for angle of internal friction is shown in Figure 11. Floor heave initiated near average peak pillar stress and would be visually detectable as rib shortening reaches about 50.8 cm (20 in). Unlike the previous case, the highest point of floor heave starts and remains at the center of the entry as shown in Figure 12. In this and preceding examples, floor heave occurred near the pillar rib for angles of internal friction of 8° or less and at the

center of the entry for an angle of internal friction greater than 8°.

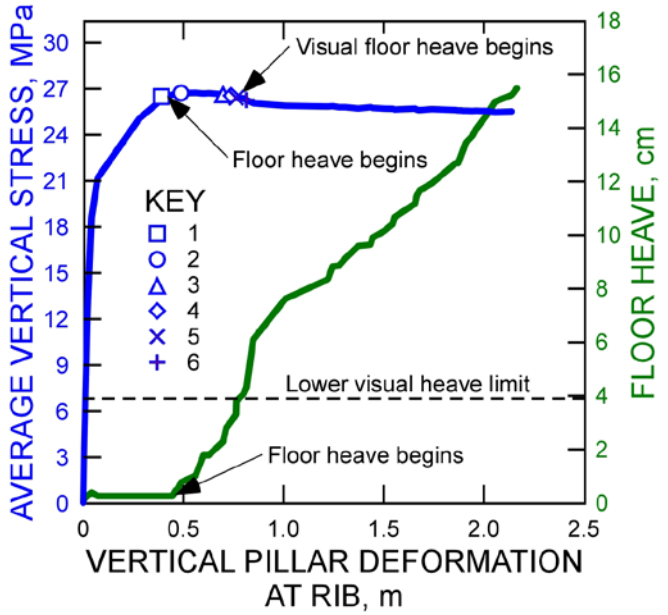

Fig. 9. Floor heave and average vertical stress versus vertical pillar deformation for a 52.4-m (172-ft) wide pillar. Floor properties are 11.72 MPa (1700 psi) for cohesion, 5° for angle of internal friction, and 9.79 GPa (1.42 x 10^6 psi) for Young's modulus.

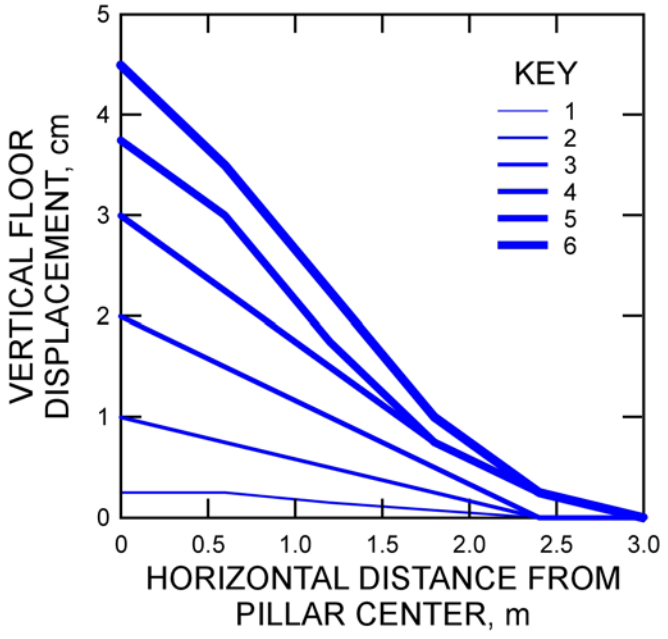

Fig. 10. Vertical displacement of floor adjacent to 52.4-m (172-ft) wide pillar as viewed from center of entry. Pillar properties are 11.72 MPa (1700 psi) for cohesion, 5° for angle of internal friction, and 9.79 GPa (1.42 x 10^6 psi) for Young's modulus.

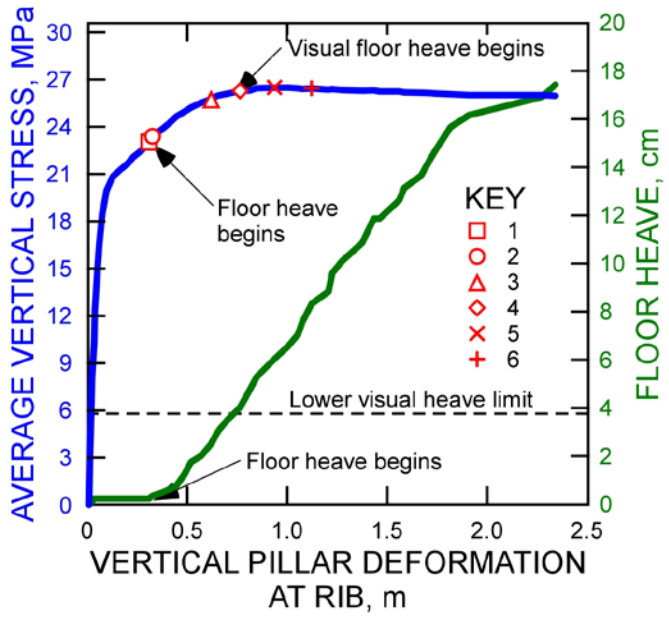

Fig. 11. Floor heave and average vertical stress versus vertical pillar deformation for a 52.4-m (172-ft) wide pillar. Floor properties are 3.4 MPa (500) psi for cohesion, 20° for angle of internal friction, and 9.79 GPa (1.42 x 10^6 psi) for Young's modulus.

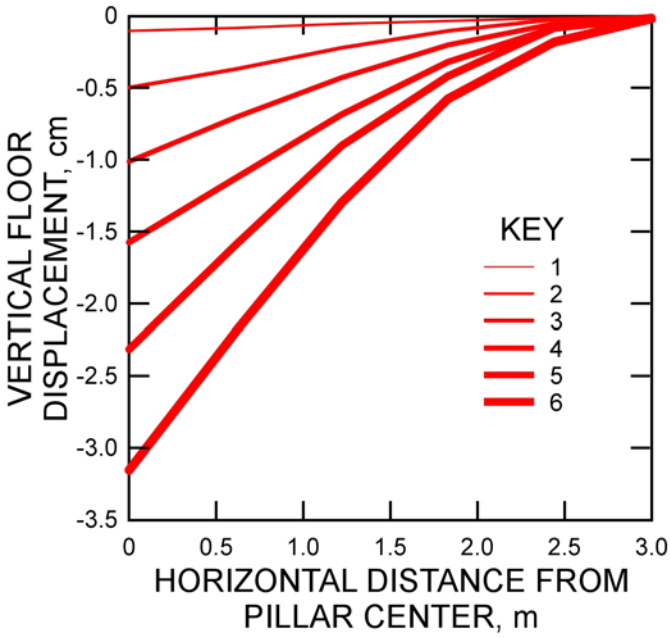

Fig. 12. Vertical displacement of floor adjacent to 52.4-m (172-ft) wide pillar as viewed from center of entry. Floor properties are 3.4 MPa (500 psi) for cohesion, 20° for angle of internal friction, and 9.79 GPa (1.42 x 10^6 psi) for Young's modulus.

4.5 Case 5: Squat pillar, floor UCS of 21.64 MPa (3139 psi), cohesion of 6.89 MPa (1000 psi), friction angle of 25 degrees

As the floor gets stronger, heave is suppressed as deformation is contained within the pillar (Figure 13). In this case, floor cohesion and angle of internal friction were 6.89 MPa (1000 psi) and 25°, respectively. Pillar

capacity increased from 26.57 MPa (3854 psi) as shown in Figure 11, to 27.59 MPa (4001 psi) as shown in Figure 13.

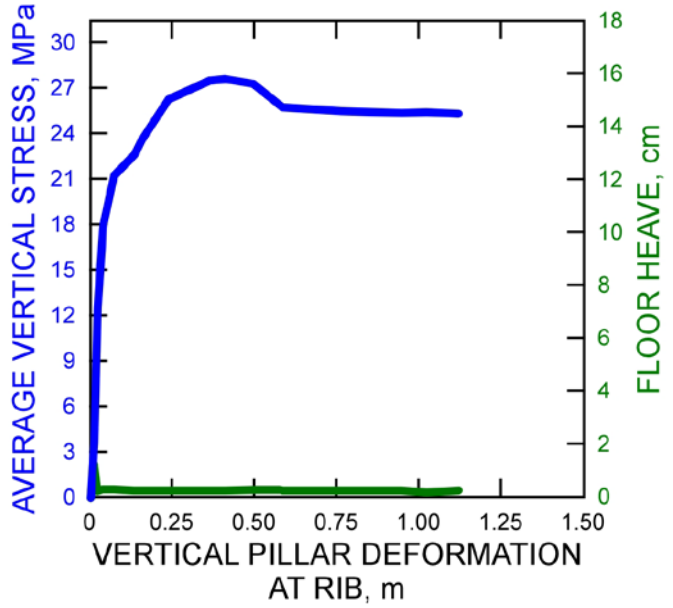

Fig. 13. Average vertical stress versus vertical pillar deformation for a 52.4-m (172-ft) wide pillar with no visual floor heave [heave less than 3.8 cm (1.5 in)]. Floor properties are 6.89 MPa (1000 psi) for cohesion, 25° for angle of internal friction, and 9.79 GPa (1.42 x 10^6 psi) for Young's modulus.

5. INFERRING MINE FLOOR PROPERTIES

A number of floor property cases, including examples discussed in the previous section, were run to create maps of floor behavior for intermediate, 23-m (76-ft) wide, and squat 52.4-m (172-ft) wide) pillars. The first objective was to map a region where intermediate pillars would deform without floor heave while squat pillars would deform with floor heave. The apparent relationship between floor heave location and friction angle was used to further define floor property regions.

Boundary lines that separate floor heave from no floor heave are plotted in Figure 14 for the two pillar sizes. The property set that results in floor heave for 23-m (76-ft) wide pillars is below the red line and the property set that results in no floor heave for this pillar size is above the red line. The property set that results in floor heave for 52.4-m (172-ft) wide pillars is below the blue line and the property set that results in no floor heave for this pillar size is above the blue line. The property set between the two lines satisfies floor heave for the 52.4-m (172-ft) wide pillars and no floor heave for the 23-m (76-ft) wide pillars.

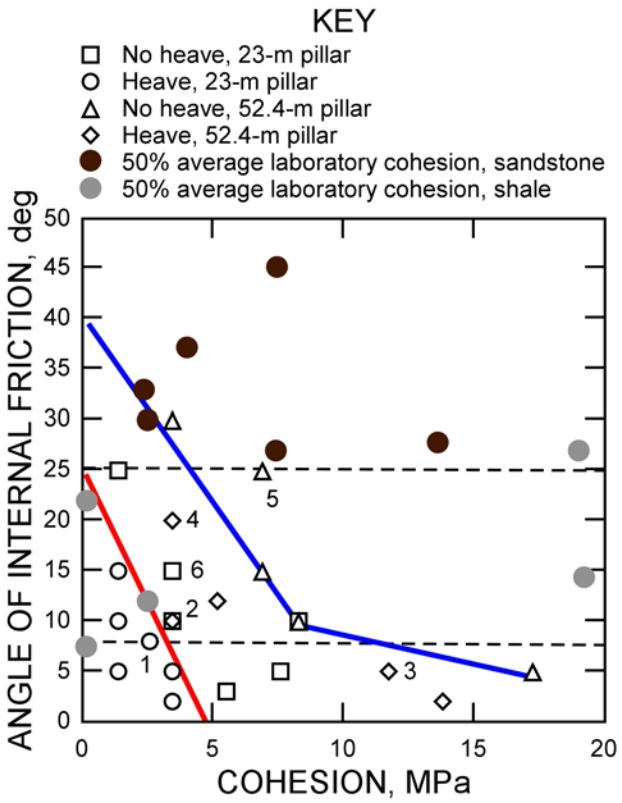

Fig. 14. Mine floor property set domain based on floor heave presence and characteristics. Cases discussed individually are marked with numbers. The 8 degree criterion for location of floor heave is also marked. Cohesion properties after Goodman [28], Sheorey [29], and Blyth and de Freitas [30].

Observations of heave location can further define floor properties. In this case, heave of the entry floor mid-point indicates the region above the 8 degree line. Finally, results can be further bounded by comparing descriptions of floor geology with reported values, in this case shale, for which average friction angles rarely exceed 25 degrees [28, 29, 10, 30], suggesting another bound. Given these bounds, a reasonable estimate of floor properties (assuming the calibrated coal properties) would seem to be a cohesion of 3.4 MPa (500 psi) and friction angle of 15°. This result is marked as "case 6" in Figure 14. Thus, the "inferred" properties combine these strength parameters with the "shale" elastic and density properties discussed earlier, as summarized in Table 2.

Table 2. Selected floor properties for point within inferred floor property boundary. Point is labeled as 6 in Fig. 14.

Parameter	Value
UCS	8.98 MPa (1303 psi)
Tensile strength	896 KPa (130 psi)
Young's modulus	9.79 GPa (1.42 x 10^6 psi)
Poisson's ratio	0.25
Angle of internal friction	15°
Cohesion	3.4 MPa (500 psi)
Specific density	2195 kg/m^3 (137 lb/ft^3)

5.1 Case 6, Inferred Properties, floor UCS of 8.98 MPa (1303 psi), cohesion of 3.4 MPa (500 psi), friction angle of 15 degrees

The inferred property case is similar to the second case with floor friction angle increased to 15° to lie well within the bounded region. Floor heave for the intermediate pillar size is almost completely absent, as shown in Figure 15. Yet, as shown in Figure 16, floor heave around the squat pillar size is substantial, raising the center of the entry floor (Figure 17).

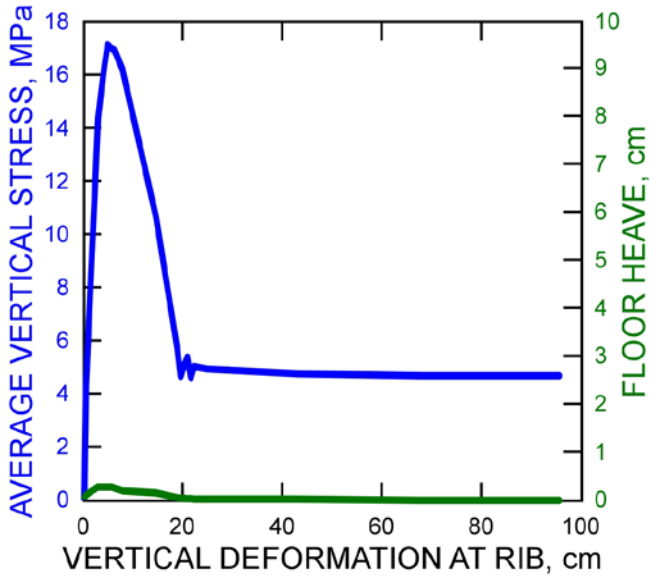

Fig. 15. Average vertical stress versus vertical pillar deformation for a 23-m (76-ft) wide pillar with no visual floor heave [heave less than 3.8 cm (1.5 in)]. Floor properties are 3.4 MPa (500 psi) for cohesion, 15° for angle of internal friction, and 9.79 GPa (1.42 x 10^6) psi for Young's modulus.

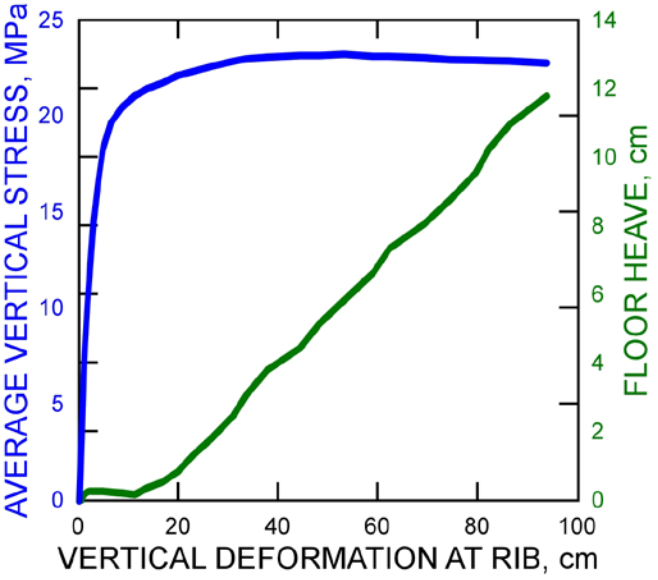

Fig. 16. Average vertical stress versus vertical pillar deformation for a 52.4-m (172-ft) wide pillar with floor heave. Floor properties are 3.4 MPa (500 psi) for cohesion, 15° for angle of internal friction, and 9.79 GPa (1.42 x 10^6) psi for Young's modulus.

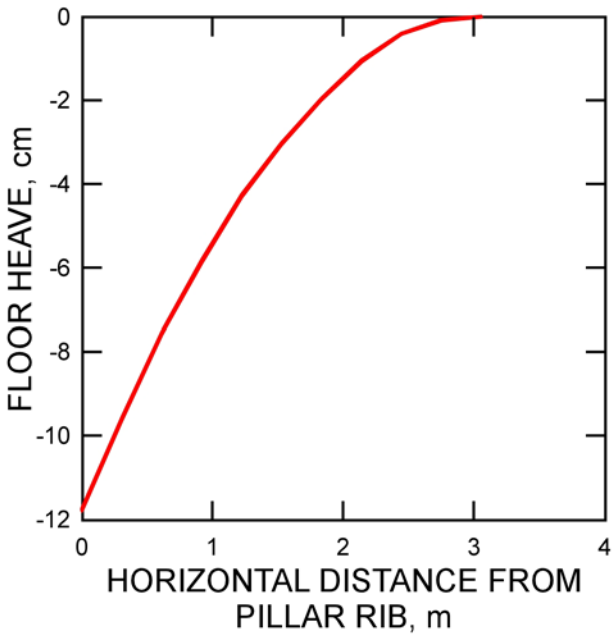

Fig. 17. Vertical displacement of floor adjacent to 52.4-m (172-ft) wide pillar as viewed from center of entry. Floor properties are 3.4 MPa (500 psi) for cohesion, 15° for angle of internal friction, and 9.79 GPa (1.42 x 10^6) psi for Young's modulus. Rib deformation is about 1 m (3 ft).

6. PILLAR SHAPE EFFECTS

The calibrated coal model, with an elastic floor and both strong and inferred floor strength, was run for a variety of shapes. These included width-to-height ratios from 1.82 to 16.36 (Figure 18). There was limited yielding in a modeled "strong" floor except for pillar width-to-height ratio of 1.82, in which there was no floor failure. Pillar stress versus strain plots for all width-to-height ratios were identical to the "elastic roof and floor" cases in Figure 18. A similar set of models were run to explore shape effects for the "inferred" floor properties. Pillars with shape ratios from 1.82 to 12 exhibited strain softening that transitioned to elastic-perfectly plastic at 16 for both the strong floor case and for a point chosen within the inferred property zone. The plot for width-to-height of 16.36 hardened after the initial peak, and then failed with "bad geometry".

A mine floor with "inferred" properties reduced pillar capacity for pillar width-to-height ratios from 4 to 12 by 5-20% compared to pillars having an elastic roof and floor as shown in Figure 18. Reductions are 10-37% by comparison to a simple linear extrapolation of the Bieniawski equation.

7. PILLAR CAPACITY EQUATIONS

A variety of equations have been proposed for estimating the variation in pillar capacity with shape. A collection of these were summarized in normalized form by Mark [31], reproduced here in Figure 19 along with results from Figure 18. The figure includes an additional

equation proposed by Maleki [32] for deep western coal mines that is the most conservative for squat pillars. An interesting feature of this figure is how all curves have a relatively linear straight shape for slender pillars where data is available but have widely differing shapes when extrapolating to squat pillars. Indeed, Mark [31] comments that "the strength of squat pillars can vary considerably depending upon the presence of soft partings, weak roof or floor interfaces, and other geologic factors" and more research is needed. In fact, the Bieniawski equation was originally recommended only for pillar width-to-height ratios up to 5 [6]. Subsequent work [33] extended this to 12, but this extension was based on sparse data [34] with considerable scatter, especially for ratios above 8, with an overall r^2 of 0.25.

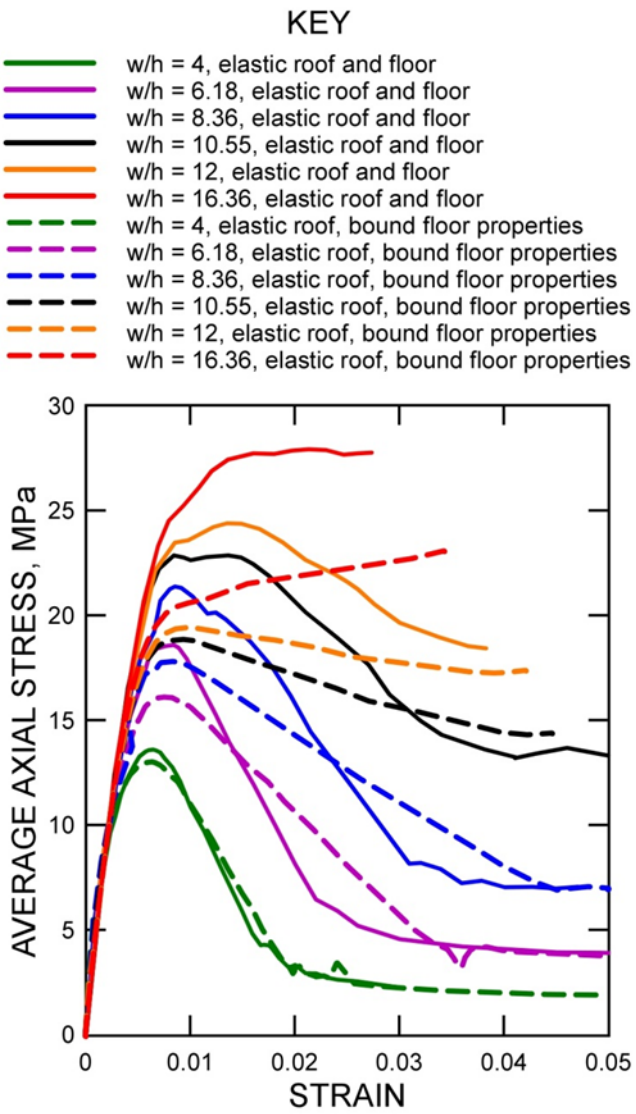

Fig. 18. Pillar stress versus strain plots created by using Hoek-Brown parameters calibrated to Bieniawski's in situ test. Dashed curves show the effect of a weakened floor.

Pillar capacity results from Figure 18 are plotted in Figure 20 along with the capacity of a 52.4-m (172-ft) wide pillar from Figure 16. The capacity for a 52.4-m (172-ft) wide pillar calculated from the equation fit to the "elastic roof and floor" case is 27.94 MPa (4053 psi) compared to 42.4 MPa (6149 psi) when Bieniawski's equation is used, resulting in a reduced capacity of 34%. The fit equation for the inferred floor properties yields 22.68 MPa (3290 psi), or another 12%, for a total reduction of 46% lower than a linear extrapolation of Bieniawski's equation.

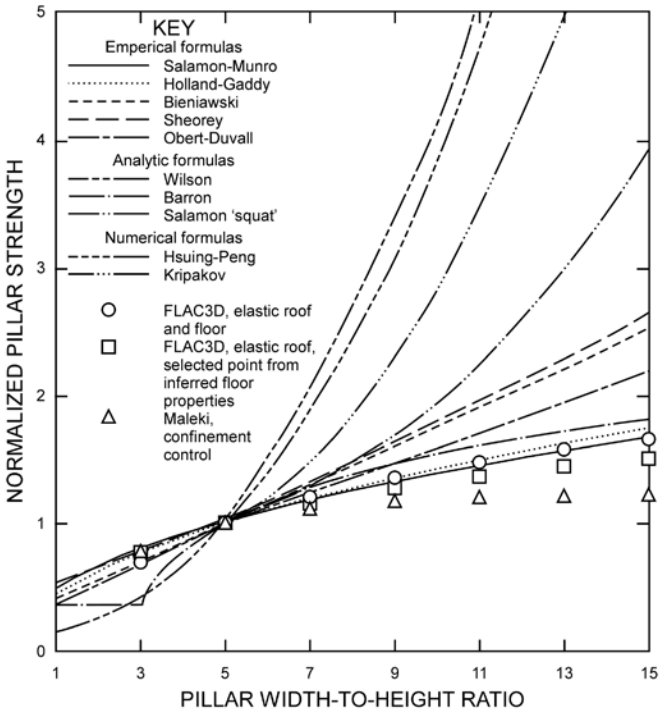

Fig. 19. Normalized pillar strengths (after Mark [31]) with results from Fig. 4 and Maleki [32]. Strong and inferred floor shape effects closely match the Holland-Gaddy equation.

The Holland-Gaddy equation fit to these data, along with the Bieniawski curve discussed earlier are also shown. These model pillar capacities are easily fit by the Holland-Gaddy form of pillar capacity equation [35], which has the form:

$$\sigma_p = \frac{k\sqrt{w}}{h} \quad (3)$$

Where:

k = Gaddy constant [36] defined in Eq. (4)

w = pillar width m (in)

h = pillar height m (in)

σ_p = pillar strength N/m^2 (lb/in^2)

$$k = S_c\sqrt{d} \quad (4)$$

Where:

S_c = coal specimen strength N/m^2 (lb/in^2)

d = side length of specimen cube m (in)

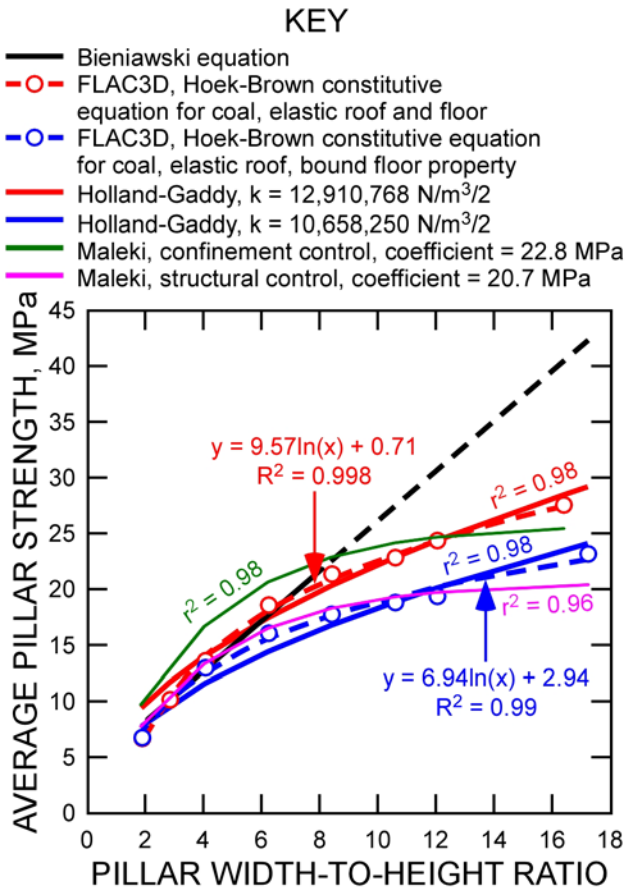

Fig. 20. Maximum average pillar stress versus pillar width-to-height ratio using Bieniawski's pillar capacity equation, a FLAC3D numerical model with parameters in the Hoek-Brown constitutive equation calibrated to Bieniawski's in situ compression test, the Holland-Gaddy pillar equation, and the Maliki pillar equations.

The value of k in the Holland-Gaddy equation is 12,910,768 N/m$^{3/2}$ (11,750 lb/in$^{3/2}$) for the case of an elastic floor and roof, and 10,658,250 N/m$^{3/2}$ (9700 lb/in$^{3/2}$) for the case of an elastic roof and weak floor. Holland [35] reported k values ranging from 5,301,655 N/m$^{3/2}$ to 11,647,160 N/m$^{3/2}$ (4825 lb/in$^{3/2}$ to 10,600 lb/in$^{3/2}$), and Lawall and Holland [37] reported k equal to 5,631,292 N/m3/2 (5125 lb/in$^{3/2}$) as listed in Table 3. The value of k for the inferred floor property case differs by only of 8% from the maximum reported value of k reported by Holland [35] for the Marker coal bed in the Pittsburgh seam.

Table 3. Values of k for the Holland-Gaddy pillar equation.

Group Name	k (N/m$^{3/2}$)	k (lb/in$^{3/2}$)
West Virginia coal [37]	5,631,292	5125
Pittsburgh coal seam [35]	6,099,376	5551
Clintwood coal seam [35]	5,301,655	4825
Marker coal seam [35]	11,647,160	10,600
FLAC3D, elastic roof and floor	12,910,768	11,750
FLAC3D, elastic roof, bound floor	10,658,250	9700

Maleki's pillar capacity equations (Eqs. 5 and 6) were developed primarily from data from western coal seams [32, 38]. Eq. (5) was applied to pillars in "mines with structurally controlled coal seams, including persistent cleats and in-seam contact planes" [32] and can reasonably be compared to capacities from FLAC3D models of pillars with an elastic roof and Mohr-Coulomb floor properties. The shape of this equation was used to compare pillar capacities by reducing the coefficient in Equation (5) to 20.684 MPa. The resulting equation provides more conservative pillar capacities than FLAC3D and calibrated Holland-Gaddy capacities for width-to-height ratios greater than 11 as shown in Figure 20.

$$\sigma_p = 26.448(1 - e^{-0.26\frac{w}{h}}) \quad (5)$$

Where:

σ_p = pillar strength (MPa)

w = pillar width (m)

h = pillar height (m)

Eq. (6) is Maleki's pillar capacity equation for mines having pillars with a large degree of confinement and can reasonably be compared to capacities from FLAC3D pillar models with an elastic roof and floor by reducing the coefficient to 22.753 MPa. The resulting equation provides more conservative pillar capacities than FLAC3D and calibrated Holland-Gaddy capacities for width-to-height ratios greater than 9.

$$\sigma_p = 32.405(1 - e^{-0.339\frac{w}{h}}) \quad (6)$$

Where:

σ_p = pillar strength (MPa)

w = pillar width (m)

h = pillar height m (m)

CONCLUSIONS

A new method for inferring relative floor properties from observations of the presence and pattern of floor heave around pillars of different sizes has been presented and demonstrated. The method is particularly valuable for extrapolating the capacity of squat pillars, which this study shows may have half the capacity suggested by a simple linear extrapolation of pillar capacity equations. Moreover, this method ensures consistency between observed and modeled ground response, particularly the presence and characteristics of floor heave. Such correlations between model and behavior serve to develop confidence in modeling as a design tool. Similarly, loss of this correlation might suggest that design model assumptions no longer hold and that the design should be reviewed.

The method applies where the presence of floor heave depends on pillar size, as has been observed in a deep western U.S. longwall coal mine. In this case, floor heave was observed near pillars approximately 52.4 m (172 ft) wide but was absent around pillars approximately 23 m (76 ft) wide, as the longwall passed.

The method idealizes pillars in FLAC3D models as a single square column that includes the roof, pillar, and floor. This idealization is similar to the force-deformation curves used to characterize pillars in boundary element models. This proof-of-concept model could easily be extended to include rectangular pillars and other local details. Coal in mine pillars was modeled as a Hoek-Brown material. Parameters were tuned to match one of Bieniawski's in situ compression tests on a square block. FLAC3D pillar capacities using tuned parameters replicated pillar capacity estimates from the Bieniawski pillar strength equation with an unconfined compressive strength of 6.2 MPa (900 psi) for pillar width-to-height ratios up to 8. Mohr-Coulomb properties in the floor were then varied to define a boundary between heave and no-heave floor response to loading for each pillar size. The intersection of these solution sets served to bound Mohr-Coulomb properties for the mine floor.

This method was also used to explore the character of floor heave, which is also readily observed underground. Heave of the pillar rib boundary, relative to the center of the entry, was characteristic of weak floors with low friction angles. Heave at the center of the entry required a friction angle of at least 8 degrees. These observations and reported shale properties were used to infer floor properties of 3.4 MPa (500 psi) cohesion and 15 degrees friction angle.

The model was then used to extrapolate capacity for a 52.4-m (172-ft) wide pillar, which had a width-to-height ratio of 17. The extrapolated capacity, for a strong roof and floor, was 34% lower than a linear extrapolation generated from Bieniawski's equation. The inferred floor properties decreased pillar capacity a further 12%—to a value about half that given by a linear extrapolation. Both results are easily fit to the Holland-Gaddy equation, with k values of 12,910,768 $N/m^{3/2}$ and 10,658,250 $N/m^{3/2}$ (11,750 $lb/in^{3/2}$ and 9700 $lb/in^{3/2}$), respectively. These results bracket those reported by Holland for the Marker coal bed in the Pittsburgh seam. Similarly, Maleki's equations can be fit to the data and provide additional conservationism for capacities of squat pillars. As such, extrapolation using numeric model results combined with empirical equations might provide a more realistic, and more conservative, estimate of squat pillar strength. Moreover, this extrapolation rests, in part, on actual observations of entry floor behavior and, in another part, on the physics of the component materials, albeit simplified.

While the applicability of this method is limited to mines in which changes in floor behavior are readily observed as pillar shapes change, its approach should be more generally applicable. That is, an estimate of pillar capacity should take full advantage of local observations of entry deformation, coal and strata characteristics, etc. Moreover, initial design models should be calibrated and verified through, at least, readily observable characteristics of ground deformation. Extrapolation of textbook equations and strength values to new locations and pillar shapes should be considered as the most tentative of estimates.

Simplifications used in this paper were used to demonstrate a procedure for inferring properties for a floor composed of one material or a composite floor represented by the behavior of one material. The resulting properties can be used as initial input in mine-wide models. These models may include additional details such as mine geology, in situ stress, mining sequence, and rockmass discontinuities where thesr control ground response to mining. The final design model must also be calibrated to instrument data that describes rockmass displacement and stress changes with mine excavation.

DISCLAIMER

The findings and conclusions presented in this document have not been formally disseminated by the National Institute for Occupational Safety and Health and should not be construed to represent any agency determination or policy. Mention of any company name or product does not constitute endorsement by NIOSH.

ACKNOWLEDGEMENTS

The authors wish to express their appreciation to Eric Zahl, civil engineer, and Heather Lawson, physical scientist, National Institute for Occupational Safety and Health (NIOSH) Office of Mining Safety and Health Research (OMSHR) for providing detailed descriptions of their visual observations of ground behavior in a deep western U.S. longwall coal mine.

REFERENCES

1. Mark, C. 1990. *Pillar design methods for longwall mining*. U.S. Department of Interior, U.S. Bureau of Mines, IC 9247.

2. Mark, C. and T. Barton. 1996. The uniaxial compressive strength of coal: Should it be used to design pillars? In *Proceedings of the 15th International Conference on Ground Control in Mining, Golden, 13-15 August 1996*. 6547-6559. Golden: Colorado School of Mines.

3. Lawson, H., J. Whyatt, and E. Zahl. 2011. Ground condition Mapping: A Case Study. In *2011 SME*

Annual Meeting and Exhibit, Denver, 27 February – 2 March, 2011 Preprints, 9 pp. Englewood: SME.

4. Karabin, G.J and M.A. Evanto. 1994. Experience with the boundary element method of numerical modeling as a tool to resolve complex ground control problems. In *Proceedings of the 13th International Conference on Ground Control in Mining, Morgantown, 2-4 August 1994,* eds. S.S. Peng et al, 201-213. Morgantown: West Virginia University.

5. Skiles, M.E. and K.G. Striklin. 2009. *U.S. Department of Labor, Program Information Bulletin No. P09-03*.

6. Bieniawski, Z.T. and W.L. Van Heerden. 1975. The significance of in situ tests on large rock specimens. *Int. J. Rock Mech. & Min. Sci.* 12: 101-113.

7. Vesic, A.S. 1975. Bearing capacity of shallow foundations. In *Foundation Engineering Handbook,* eds. H.F. Winterkorn et al., 121-147.

8. Gadde, M.M. 2011. The applicability of the Vesic-Speck floor bearing capacity model to size pillars in the Illinois basic coal mines. *In Proceedings of the 45th U.S. Rock Mechanics/Geomechanics Symposium, San Francisco, 26-29 June 2011*.

9. Su, D.W. and G.J. Hasenfus. 1999. Coal Pillar strength and practical coal pillar design considerations. In: *Proceedings of the second international workshop on coal pillar mechanics and design, Vail, 6 June 1999,* eds. C. Mark et al., 155-162. U.S. Department of Health and Human Services IC 9448.

10. Hajsdarwish, A. and A. Shakoor. 2006. Predicting the shear strength parameters of mudrocks. In *Proceedings of the 10th IAEG Congress, Nottingham, 6-10 September 2006,* 7 pp. London: The Geological Society of London.

11. Heasley, K. A. 1998. *Numerical Modeling of Coal Mines with a Laminated Displacement-Discontinuity Code.* Ph.D. Dissertation. Golden: Colorado School of Mines.

12. Zipf, R. K., Jr. 1992. *MULSIM/NL Theoretical and Programmer's Manual.* USBM Information Circular 9321.

13. Itasca Consulting Group. 2009. FLAC3D: Fast Lagrangian Analysis of Continua in 3 Dimensions-User's Guide (Version 4.0).

14. Yang, T. 1991. Influence of specimen size and shape on the strength of coal. *MS Thesis, University of Alberta.*

15. Scovazzo, V.A. 2010. Analytical design procedure using the Wilson Equation. In *2010 SME Annual Meeting and Exhibit, Phoenix, 28 February – 3 March, 2010 Preprints,* 6 pp. Englewood: SME.

16. Kalamaras, G.S. and Z.T. Bieniawski. 1993. A rock mass strength concept for coal seams. In Proceedings of the 12th International Conference on Ground Control in Mining, Morgantown, 3-5 August 1994, 274-283. Morgantown: West Virginia University.

17. Hoek, E., C. Carranza-Torres, and B. Corkum. 2002. In *Proceedings of the 5th North American Rock Mechanics Symposium.Toronto, 7 – 10 July 2002,* eds. R. Hammah et al, 267-273. Toronto: U. of Toronto Press.

18. Duncan Fama, M.E., R. Trueman, and M.S. Craig. 1995. Two- and three-dimensional elasto-plastic analysis for coal pillar design and its application to highwall mining. *Int. J. Rock Mech. & Min. Sci. 32: 215-225.*

19. Obert, L. and W.I. Duvall, W.I. 1967. *Rock Mechanics and the Design of Structures in Rock.* New York: Wiley.

20. Salamon, M.D.G. and A.H. Monroe. 1967. A study of the strength of coal pillars. *J. S. Afr. Inst. Min. Metall.* 68: 55-67.

21. Jaiswal, A. and B.K. Shrivastava. 2009. Numerical simulation of coal pillar strength. *Int. J. Rock Mech. & Min. Sci.* 46: 779-788.

22. Jaiswal, A. and B.K. Shrivastva. 2012. Stability analysis of the proposed hybrid method of partial extraction for underground coal mining. *Int. J. Rock Mech. & Min. Sci.* 52: 103-111.

23. Esterhuizen, E., C. Mark, and M.M. Murphy. 2009. Numerical model calibration for simulating coal pillars, gob, and overburden response. In *Proceedings of the 29th International Conference on Ground Control in Mining, Morgantown, 27-29 July 2010,* 12 pp.

24. Mark, C. and F. Chase. 1977. Analysis of Retreat Mining Pillar Stability. In *Proceedings, New Technology for Ground Control in Retreat Mining.* 35-38. NIOSH IC 9446.

25. Pariseau, W.G. 2012. *Design Analysis in Rock Mechanics,* 2nd ed. Leiden: Balkema.

26. Farmer, I.W. 1968. *Engineering properties of rocks.* London: Butler and Tanner.

27. Wilson, A.H. and D.P. Ashwin. 1972. Research into the determination of pillar size. *The Mining Engineer,* Volume 131, Part 9, Number 141: 409-417.

28. Goodman, R.E. 1989. *Introduction to Rock Mechanics,* 2nd ed. New York: John Wiley & Sons.

29. Sheorey P.R. 1997. *Empirical Rock Failure Criteria*. Rotterdam: A.A. Balkema.

30. Blyth, F.G.H. and H.H. de Freitas. 1984. *A Geology for Engineers.* New York: Elsevier.

31. Mark, C. 2006. The evolution of intelligent coal pillar design: 1981-2006. In *Proceedings of the 25th International Conference on Ground Control in Mining, Morgantown, 1-3 August 2006,* eds. S.S. Peng et al., 325-334.

32. Maleki, H. 1992. In situ pillar strength and failure mechanisms for U.S. coal seams. In *Proceedings of International Conference on Coal Pillar Design and Mechanics, Santa Fe, 1992,* 73-77. USBM IC 9315.

33. Bieniawski, Z.T. 1992. A method revisited: Coal pillar strength formula based on field investigations. In *Proceedings of the Workshop on Coal Pillar Mechanics and Design*, eds. A.T. Iannacchione et al, 158-165. Bureau of Mines Information Circular 9315.

34. Mark, C., J. Listak, and Z.T. Bieniawski. 1988. Yielding coal pillars – field measurements and analysis of design methods. In *Proceedings of the 29th U.S. symposium on Rock Mechanics, University of Minnesota, June 1988*, eds. P.A. Cundall et al, 261-270. Rotterdam: Balkema.

35. Holland, C.T. 1964. The strength of coal in mine pillars. In *Proceedings of the 6th Symposium on Rock Mechanics, University of Missouri, Rolla, October 1964*, eds. E.M. Spokes et al, 450-466. Rolla: The University of Missouri at Rolla.

36. Gaddy, L.F. 1956. A study of the ultimate strength of coal as related to the absolute size of the cubical specimens tested. *Bulletin of the Virginia Polytechnic Institute, Engineering Experiment Station Series No. 112,* 27 pp.

37. Lawall, C.E. and C.T. Holland. 1937. *Some physical characteristics of West Virginia Coals.* Morgantown: West Virginia University Bulletin, Series 37, No. 8-IV.

38. Maleki, H. and J.C. Lewis. 2010. Verification of in situ pillar strength for Utah coal seams. In *Proceedings of the 44th US Rock Mechanics Sympsoium and 5th U.S.-Canada Rock Mechanics Symposium, Salt Lake City, June 27-30, 2010,* 15 pp. American Rock Mechanics Association.